

Are rapid changes in brain elasticity possible?

K J Parker

Department of Electrical and Computer Engineering, University of Rochester,
Hopeman Building 203, PO Box 270126, Rochester, NY 14627-0126,
United States of America

Email: kevin.parker@rochester.edu

Received 2 May 2017, revised 20 July 2017

Accepted for publication 2 August 2017

Published 1 September 2017



CrossMark

Abstract

Elastography of the brain is a topic of clinical and preclinical research, motivated by the potential for viscoelastic measures of the brain to provide sensitive indicators of pathological processes, and to assist in early diagnosis. To date, studies of the normal brain and of those with confirmed neurological disorders have reported a wide range of shear stiffness and shear wave speeds, even within similar categories. A range of factors including the shear wave frequency, and the age of the individual are thought to have a possible influence. However, it may be that short term dynamics within the brain may have an influence on the measured stiffness. This hypothesis is addressed quantitatively using the framework of the microchannel flow model, which derives the tissue stiffness, complex modulus, and shear wave speed as a function of the vascular and fluid network in combination with the elastic matrix that comprise the brain. Transformation rules are applied so that any changes in the fluid channels or the elastic matrix can be mapped to changes in observed elastic properties on a macroscopic scale. The results are preliminary but demonstrate that measurable, time varying changes in brain stiffness are possible simply by accounting for vasodynamic or electrochemical changes in the state of any region of the brain. The value of this preliminary exploration is to identify possible mechanisms and order-of-magnitude changes that may be testable *in vivo* by specialized protocols.

Keywords: brain, viscoelastic models, MRE, shear waves

(Some figures may appear in colour only in the online journal)

1. Introduction

While elastography of different organs is growing in terms of technology and clinical applications (Parker *et al* 2011), a particular area of research emphasis is the brain and possible links between neuropathology and altered viscoelasticity. A common clinical goal across elastography is to determine what clinical conditions can be detected or followed progressively by measurable changes in tissue stiffness and shear wave speed. In the brain, research studies have assessed the elastic properties of the normal brain including regional and grey/white matter differences, and for pathologies including Alzheimer's disease, and multiple sclerosis. A recent summary of many magnetic resonance elastography (MRE) studies is given in Hiscox *et al* (2016). In addition to MRE, ultrasound studies of brain elasticity are under investigation. A transcranial assessment of brain pulsatility has shown correlations with disease states (Desmidt *et al* 2011, Ternifi *et al* 2014). Furthermore, shear wave elastography has shown promising utility for intraoperative uses (Chan *et al* 2014, Chauvet *et al* 2016).

One feature of brain elastography research is the wide range of values measured and reported within categories, and Hiscox *et al* conclude that 'providing standardized baseline values for the brain is very challenging'. Methodology plays a role here as does choice of parameters including the shear wave frequency, commonly in the range of 50 - 80 Hz. However, there is a possibility that the unique structure and function of the brain enable dynamic changes in regional elasticity (viscoelastic properties, complex modulus, and shear wave speed) over a time scale from many seconds to minutes (Patz *et al* 2016). For example, at shear wave frequencies of 1 kHz in the mouse brain, Patz *et al* (2017a) have reported regional increases of 14% in shear modulus during neuronal activation. If dynamic changes are possible and are of significant magnitude, then they could influence experiments where these effects are not recognized and are not controlled, thus contributing to a wide variation in experimental results. Conversely, if dynamic changes in brain elasticity are possible and are of significant magnitude, then they may be experimentally activated or controlled, and the resulting effects could add useful clinical information.

For this reason, an examination of hypothetical dynamic changes in brain elasticity is warranted. This paper provides a preliminary assessment of three conditions that could, in principle, rapidly alter elastic measures: vasodilation within an organ that is unconfined, vasodilation within a strictly confined volume (such as the skull), and changes in the elastic matrix of the tissue. All three cases are examined using the microchannel flow model and a general transformation rule that gives an expression for the elastic response of tissue in a modified state.

2. Theory

2.1. Review of theory

The microchannel flow model (Parker 2014) begins with consideration of a block of tissue, comprised of a multi-scale interlocking of cells, connective tissue, and a variety of fluid channels. To analyze the structural element, an idealized cube of tissue with only one vessel of radius r is supported at the base and subjected to uniaxial loading. If the fluid within a microvessel of length L experiences a pressure drop due to the applied stress σ_x , then under Poiseuille's Law for incompressible fluids in pipes, a volumetric flow rate Q will result (Sutera 1993):

$$Q = \frac{C\sigma_x r^4}{\eta} \quad (1)$$

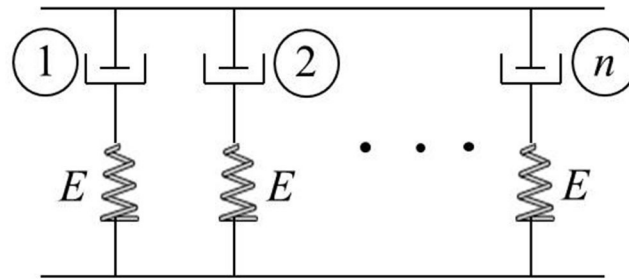


Figure 1. The microchannel flow model of perfused soft tissue begins with parallel elements (Parker 2014). Each dashpot corresponds to a fluid-filled vessel or channel, with the smallest microchannel yielding the largest time constant, via Poiseuille’s Law. In the continuing limit, the aggregate sum over the fractal size distribution yields the microchannel flow model. Reproduced from Parker *et al* 2014. © 2014 Institute of Physics and Engineering in Medicine. All rights reserved.

where C is a constant, r is the radius of the microvessel, and η is the viscosity of the fluid. Accounting for the loss of fluid from the vessel and combining elastic and fluid outflow strains as additive leads to a Maxwell model of a series spring and dashpot, therefore the stress relaxation (SR) curve is a simple exponential decay. If $\varepsilon(t) = \varepsilon_0 U(t)$, where $U(t)$ is the unit step function, then

$$\sigma_{\text{SR}}(t) = \varepsilon_0 E e^{-t/\tau} \text{ for } t \geq 0, \tag{2}$$

where E is the Young’s modulus of the elastic parenchyma and the time constant τ is:

$$\tau = \frac{\eta C}{E r^4}. \tag{3}$$

The inverse dependence of τ on radius to the fourth power makes the time constant exquisitely sensitive to changes in vessel radius.

Next, we assume there are n multiple microchannels of unequal radius r_n and therefore unequal flow rates Q_n . In this case, if each contributes to the stress relaxation at their respective time constant τ_n , then the simplest model for this looks like a parallel set of Maxwell elements (figure 1).

This configuration of multiple parallel elements and an optional single spring element is the generalized Maxwell-Weichert model (Ferry 1970, Fung 1981), with the time constants of each element determined by equation (3) and therefore sensitive to $1/r_n^4$. Generally, we can write the stress relaxation solution for N Maxwell elements as a Prony series (Lakes 1999), the sum of components with characteristic relaxation time constant τ_N . In the limit, as we allow a continuous distribution of time constants τ , the summation becomes an integral and $A(\tau)$ is the relaxation spectrum, which can be either discrete or continuous, depending on the particular medium under study (Fung 1981). Given a material’s $A(\tau)$, we can write:

$$\sigma_{\text{SR}}(t) = \int_0^\infty A(\tau) e^{-t/\tau} d\tau. \tag{4}$$

Now consider a specific power law distribution:

$$A(\tau) = A_0 \tau^{-b}; \quad 1 < b < 2. \tag{5}$$

The power law distribution is naturally occurring in many natural structures including normal and pathological circulatory systems (West *et al* 1997, Risser *et al* 2007). Substituting equation (5) into equation (4) and solving yields the solution:

$$\sigma_{SR}(t) = A_0 \cdot t^{1-b} \Gamma [b - 1] \text{ for } 1 < b < 2, t > 0 \tag{6}$$

where Γ is the Gamma function. The stress relaxation response is characterized by $t^{1/b-1}$ decay for $t > 0$. For values of $1 < b < 2$ this tends to have a sharp initial drop and then a slow asymptomatic decay. It can also be shown that the frequency dependence of the complex modulus is given by a power law:

$$|E(\omega)| = \frac{A_0}{\sqrt{2\pi}} \Gamma[a] \Gamma[1-a] |\omega|^a \tag{7}$$

where $a = b - 1$. This response is dominated by the steady increase with frequency to the power of a .

In practical cases it is more realistic to place limits on the range of τ for a material, reflecting the longest and shortest time constraints that pertain to the smallest to largest vessels and microchannels. In this case, the integration of equation (4) has limits τ_{min} and τ_{max} and

$$\sigma_{SR}(t) = \int_{\tau_{min}}^{\tau_{max}} A(\tau) e^{-t/\tau} d\tau \tag{8}$$

and assuming the power law form of equation (5), then

$$\sigma_{SR}(t) = A_0 \left(\frac{\Gamma \left[a, \frac{t}{\tau_{max}} \right] - \Gamma \left[a, \frac{t}{\tau_{min}} \right]}{t^a} \right) \text{ for } a > 0, t \geq 0, \text{ and } 0 < \tau_{min} < \tau_{max} \tag{9}$$

where $\Gamma [a, t/\tau]$ is the incomplete Gamma function (upper-tailed). This version of the micro-channel flow model is a four parameter model since τ_{max} and τ_{min} must be determined as material-specific parameters in addition to a and A_0 . A different closed form solution exists for cases where $a \leq 1$. The complex modulus $|E(\omega)|$ for the material of equation (9) is given in Parker, Ormachea *et al* (2016), basically this approaches a power law of equation (7), but only gradually as τ_{max} and τ_{min} are widely separated.

In summary, if a tissue has a power law relaxation spectrum $A(\tau) = A_0 \tau^{-b}$, then the stress relaxation response will show a $\sigma_{SR} \cong A_0 t^{1-b} = A_0/t^a$ response. The tissue stress-strain transfer function in the frequency domain is $|E(\omega)| \cong A_0 |\omega|^a$, and shear wave phase velocity $c_{ph}(\omega) \propto \omega^{a/2}$. In prostate and liver (Zhang *et al* 2007, Parker 2014, Ormachea *et al* 2016), $0 < a < (1/4)$ for many normal specimens.

2.2. Mapping changes from r to τ to $A(\tau)$ to $\sigma_{SR}(t)$

Given a fractal distribution of blood vessels of radius r where $r_{max} > r > r_{min}$, and a corresponding $A(\tau) = A_0/\tau^b$ from $\tau_{min} < \tau < \tau_{max}$, where the relationship between τ and r is influenced by Poiseuille’s Law (equation (3)), we now examine the new relaxation spectrum $A_2(\tau_2)$ if all the vessel radii are increased or decreased by a factor of $r_2 = \chi r$ where $\chi > 1$ represents vasodilation and $\chi < 1$ vasoconstriction. To map the changes to the relaxation spectrum function $A(\tau)$, we use the general transformation rule from probability theory (Papoulis 1987). Given a monotonic distribution $A(r)$ and a transformation $\tau_2 = C/(\chi r)^4 = \tau/\chi^4$, then the transformed density function $A_2(\tau_2)$ is given by:

$$A_2(\tau_2) = \frac{A(\tau)}{\left| \frac{d\tau_2}{d\tau} \right|}. \tag{10}$$

Substituting and taking the derivative we have

$$A_2(\tau_2) = \chi^4 A(\chi^4 \tau_2). \tag{11}$$

However, assuming $A(\tau) = A_0/\tau^b$, then

$$A_2(\tau_2) = \frac{\chi^{(4-4b)} A_0}{\tau_2^b} = \frac{\chi^{4(1-b)} A_0}{\tau_2^b}, \tag{12}$$

and this also preserves the total area under the relaxation spectrum:

$$\int_{\tau_{\min}}^{\tau_{\max}} A(\tau) d\tau = \int_{\tau_{2\min}}^{\tau_{2\max}} A_2(\tau_2) d\tau_2. \tag{13}$$

where

$$\begin{aligned} \tau_{2\max} &= C/(\chi r_{\min})^4 = (1/\chi)^4 \tau_{\max} \quad \text{and} \\ \tau_{2\min} &= C/(\chi r_{\max})^4 = (1/\chi)^4 \tau_{\min}. \end{aligned} \tag{14}$$

2.3. Proportional dilation/constriction: unconfined space

In this section we consider the relatively simple case of vasodilation (or vasoconstriction) within an *unconfined tissue* such that the extra blood volume associated with enlarged blood vessels is simply added to the organ volume.

Consider a baseline or resting state with a power law distribution of vessels between r_{\min} and r_{\max} leading to the stress relaxation spectrum

$$A(\tau) = \frac{A_0}{\tau^b} \begin{cases} \tau_{\min} \leq \tau \leq \tau_{\max} \\ \text{or} \\ \frac{C}{r_{\max}^4} \leq \tau \leq \frac{C}{r_{\min}^4}, \end{cases} \tag{15}$$

and the resulting stress relaxation function is given by equation (9). Next, assume that all vessel radii are increased or decreased by some proportion χ , where $\chi = 1$ represents the baseline case and after vasodilation or vasoconstriction:

$$r_2 = \chi r \begin{cases} \chi > 1 \text{ implies vasodilation} \\ \chi < 1 \text{ implies vasoconstriction} \end{cases}. \tag{16}$$

We apply the transformation rule to determine the new stress relaxation spectrum $A_2(\tau_2)$, where $\tau_2 = C/(r_2)^4 = C/(\chi r)^4 = (1/\chi)^4 \tau$, so $d\tau_2/d\tau = (1/\chi)^4$, and applying equation (10):

$$A_2(\tau_2) = \frac{\chi^4 A_0}{(\tau_2 \chi^4)^b} = \frac{\chi^{4(1-b)} A_0}{\tau_2^b}. \tag{17}$$

Now integrating $\int_{\tau_{2\min}}^{\tau_{2\max}} A_2(\tau_2) e^{-t/\tau_2} d\tau_2$ we find:

$$\sigma_{SR2}(t) = \frac{(\chi)^{4(1-b)} A_0 (\Gamma[a, t/\tau_{2\max}] - \Gamma[a, t/\tau_{2\min}])}{t^a} \tag{18}$$

where $\tau_{2\max}$ and $\tau_{2\min}$ are given by equation (14). Thus, equations (14) and (18) provide the transformation of elastic properties as a function of vascular changes proportional to χ , in an unconfined space.

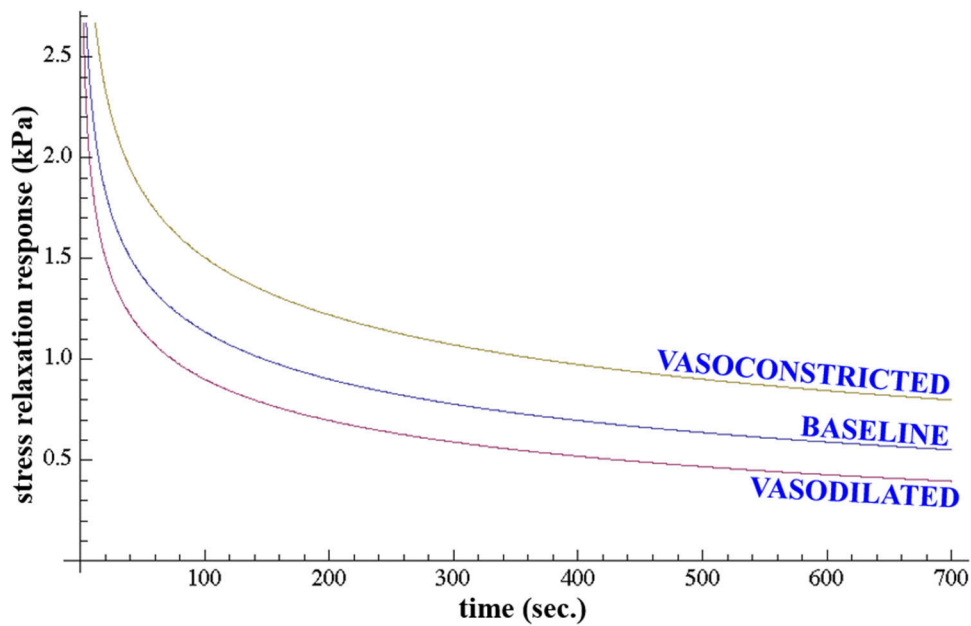


Figure 2. Stress relaxation curves in an unconfined soft tissue. Parameters are taken from table 1 with $\chi = 1.2$ or 0.8 representing vasodilation or vasoconstriction, respectively.

As an example, figure 2 shows a case where the vessels change with 20% vasodilation ($\chi = 1.2$) and then 20% vasoconstriction ($\chi = 0.8$), and using baseline parameters found in table 1. The parameters chosen are within limits seen in other soft tissues, for example 20% vasodilation is within the range of cortical blood flow changes measured by laser Doppler flowmetry during sensory stimulation (Malonek *et al* 1997).

These shifts in vessel radii create a shift in the relaxation spectrum and then a clearly observable change in stress relaxation, softening or stiffening the tissue.

The frequency domain or complex modulus is shown in figure 3, demonstrating the same trend, which would be detected in MRE as a change in shear wave speed and wavelength.

2.4. Partitioning dilation/constriction using perivascular space under constrained volume

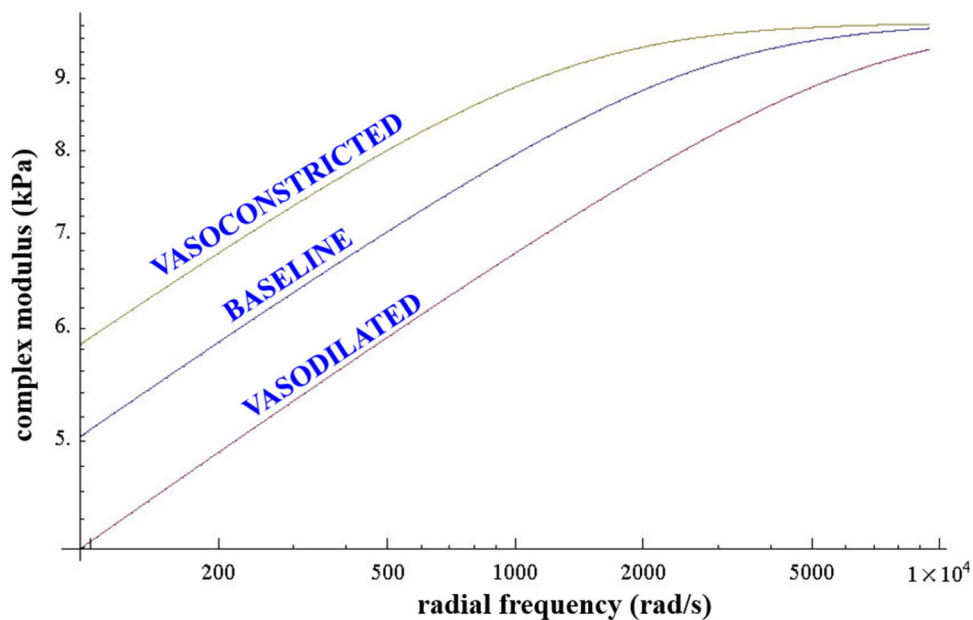
In this case, we consider the brain as a confined space such that localized vasodilation and increased blood volume must result in subtraction of an equal fluid volume. The perivascular space is one candidate for compensatory volume change (Zhang *et al* 1990). The anatomical structure of the perivascular space is shown in figure 4, suggesting an idealization as concentric tubes of negligible wall radius as idealized in figure 5.

The total volume of a vessel segment length l in figure 5 is:

$$\begin{aligned}
 V &= \underbrace{\pi l (p \cdot r)^2}_{\text{blood}} + \underbrace{\pi l \left[(r_0^2) - (p \cdot r)^2 \right]}_{\text{perivascular}} \\
 &= \pi l r_0^2,
 \end{aligned}
 \tag{19}$$

Table 1. Baseline parameters used in the microchannel flow model based roughly on other soft tissue measurements.

| Parameter | Value | Units | Comments |
|---------------|--------------------|------------------------|---|
| A | 1 | kPa | Unitary, also very soft tissue |
| $b, (a)$ | 1.2, (0.2) | Dimensionless power | Power law |
| τ_{\max} | 30,000 | s | Set by r_{\min}, C |
| τ_{\min} | 0.3 | ms | Set by r_{\max}, C |
| r_{\max} | 0.75 | mm | Tertiary branches |
| r_{\min} | 7.5 | μm | Venules |
| C | 1×10^{-4} | s mm^4 | Scale factor, empirical |
| χ | 1.2 or 0.8 | Ratio | Vasodilation or vasoconstriction |
| χ_E | 1.2 or 0.8 | Ratio | Change in elastic matrix due to electro-chemical activation |
| p_b | 0.7 | Ratio | Perivascular to vascular concentric radii |

**Figure 3.** Complex modulus vs. frequency for the three cases shown in figure 2 over a range of frequency from $2\pi \cdot 15$ Hz to $2\pi \cdot 1500$ Hz, plotted on a log–log scale.

which is independent of p , a necessary constraint in the confined volume of the brain. The partition p is a fraction $0 \leq p \leq 1$ and may exceed 0.8 in some segments of mammalian brains (Harnarine-Singh *et al* 1972, Møller *et al* 1974, Fox and Raichle 1986, Zhang *et al* 1990).

Note that the relative ratio of fluid in the perivascular space to the fluid in the vascular space (blood) is $(1 - p^2)/p^2$; for example, when $p = 0.8$, then there is a roughly equal volume of fluid in the two compartments. We will assume for simplicity that p is a constant over all branches. In this model, consistent with a constrained volume for the brain, increases in blood vessel diameters due to vasodilation require an immediate decrease in perivascular fluid to

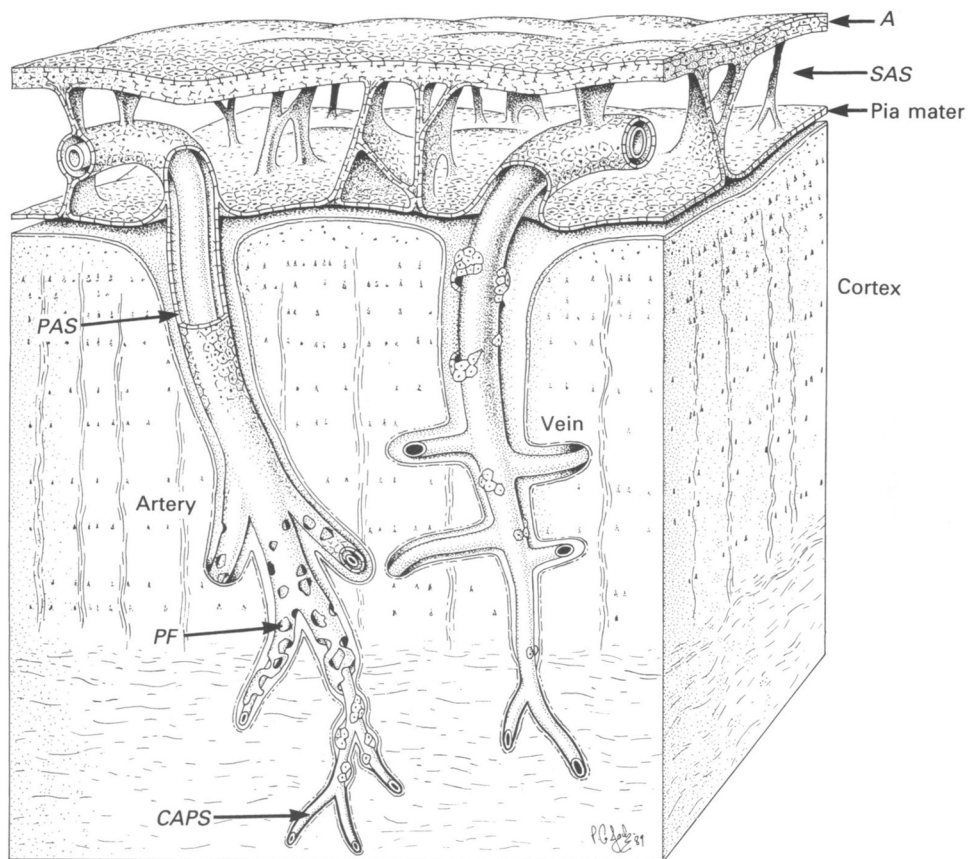


Figure 4. Diagram demonstrating the relationships of the pia mater and intracerebral blood vessels. Subarachnoid space (SAS) separates the arachnoid (A) from the pia mater overlying the cerebral cortex. An artery on the left side of the picture is coated by a sheath of cells derived from the pia mater; the sheath has been cut away to show that the periarterial spaces (PAS) of the intracerebral and extracerebral arteries are in continuity. The layer of pial cells becomes perforated (PF) and incomplete as smooth muscle cells are lost from the smaller branches of the artery. The pial sheath finally disappears as the perivascular spaces are obliterated around capillaries (CAPS). Perivascular spaces around the vein (right of picture) are confluent with the subpial space and only small numbers of pial cells are associated with the vessel wall. Diagram reused with permission: Zhang *et al* (1990) John Wiley & Sons. © 1990 Developmental Dynamics.

maintain a constant vascular and perivascular total volume. This presumes that the perivascular fluid is capable of drainage into and beyond the subarachnoidal spaces. Our focus is on the tissue response as the partitioning fraction p is changed. We postulate the superposition of two stress relaxation spectra, one for vascular and one for perivascular: $A(\tau) = A_{\text{vas}}(\tau) + A_{\text{per}}(\tau)$, linked by the fraction p as the constraint on total volume. Both are assumed to be characterized by the same power law b since they derive from the same fractal branching geometry. Furthermore, the range of diameters extends from pr_{max} to pr_{min} in the vascular network and the annular radius Δr of the perivascular network extends from $r_{\text{max}}(1-p)$ to $r_{\text{min}}(1-p)$. Finally, we assume the baseline case $A_{\text{per}}(\tau)$ is known for the perivascular spaces and $A_{\text{vas}}(\tau)$ is known for some resting baseline p_b . A more critical and detailed look at the perivascular model is given in appendix.

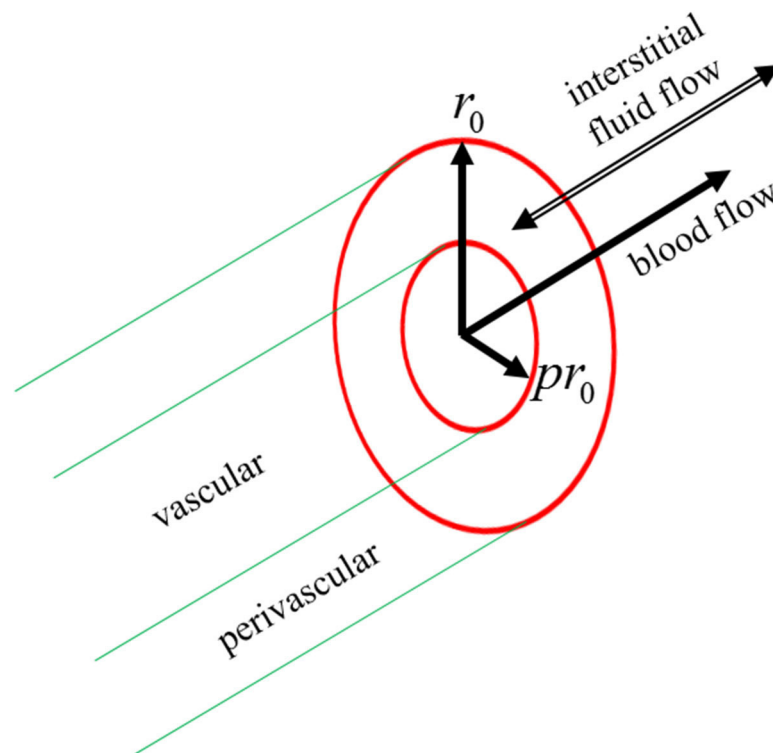


Figure 5. Partition of fluid within the vascular space (radius pr_0) and perivascular space (outer radius r_0). In vasodilation p increases but the volume of perivascular fluid must decrease to maintain constant volume in the confined brain.

Furthermore, let us assume a corresponding baseline stress relaxation function governing the macroscopic tissue either measured or estimated *a priori* as:

$$\sigma_{SR_b}(t) = A_{vas} \left(\frac{\Gamma\left(a, \frac{t}{\tau_{vmax}}\right) - \Gamma\left(a, \frac{t}{\tau_{vmin}}\right)}{t^a} \right) + A_{per} \left(\frac{\Gamma\left(a, \frac{t}{\tau_{permax}}\right) - \Gamma\left(a, \frac{t}{\tau_{permin}}\right)}{t^a} \right). \tag{20}$$

Then for vascular changes in p away from the baseline p_b , the transformation rules apply as in equation (18) where for the vascular space $\chi_{vas} = p/p_b$ and for the perivascular space $\chi_{per} = (1 - p)/(1 - p_b)$, so as one compartment increases, the other decreases. Accordingly, the new state is

$$\sigma_{SR2} = \left[\left(\frac{p}{p_b} \right)^{4(1-b)} A_{vas} \left(\frac{\Gamma\left(a, \frac{t}{\tau_{v2max}}\right) - \Gamma\left(a, \frac{t}{\tau_{v2min}}\right)}{t^a} \right) \right] + \left[\left(\frac{(1 - p)}{(1 - p_b)} \right)^{4(1-b)} A_{per} \left(\frac{\Gamma\left(a, \frac{t}{\tau_{per2max}}\right) - \Gamma\left(a, \frac{t}{\tau_{per2min}}\right)}{t^a} \right) \right], \tag{21}$$

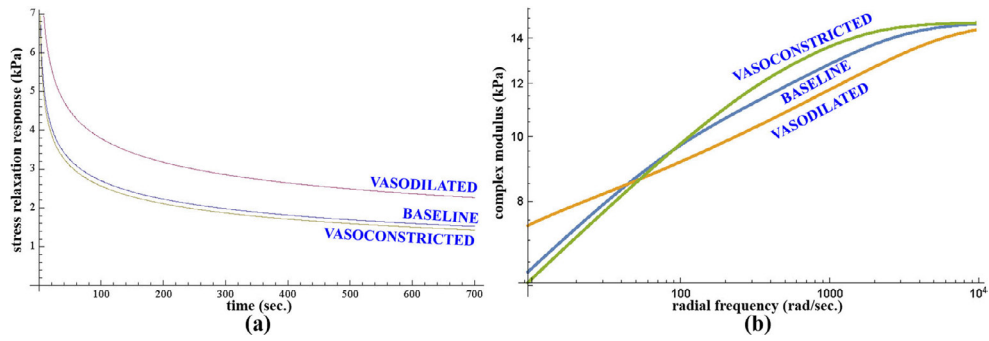


Figure 6. (a) Vasodilation under volume constraint with compensatory reduction of perivascular space dimensions. Note that the result is contrary to those in the case of an unconfined organ. This is due to the compensatory ‘squeezing’ of the perivascular space in the model. (b) Magnitude of complex modulus from radial frequencies 2π 1.5 Hz to 2π 1500 Hz, for the baseline case and vasomodulated cases assuming the perivascular network compensates for changes in the vascular space. Note that in the case of vasodilation, the ‘squeezing’ of the perivascular space leads to long time constants and a relatively high modulus at low frequencies. Thus, experimental results may also depend on shear wave frequency.

where

$$\begin{aligned} \tau_{v2} &= (p_b/p)^4 \tau_v \quad (\text{max, min}) \\ &\text{and} \\ \tau_{\text{per}2} &= ((1 - p_b)/(1 - p))^4 \tau_p \quad (\text{max, min}). \end{aligned} \tag{22}$$

Consider an example where the vascular radii of interest range as in previous examples and table 1. Assume $p_b = 0.7$ represents the resting case. Also assume a vasodilation where $p = 0.85$, so $(p/p_b)^4 = (1.2)^4 = 2.17$. Then for the perivascular space $((1 - p)/(1 - p_b))^4 = (0.5)^4 = 0.0625$. With $b = 1.2$, and assuming equal contributions for both compartments, then

$$\sigma_{\text{SR}}(t) = \frac{A_0}{t^{0.2}} \left[\left\{ \Gamma \left(0.2, \frac{t}{30\,000} \right) - \Gamma \left(0.2, \frac{t}{0.0003} \right) \right\} + \left\{ \Gamma \left(0.2, \frac{t}{940\,000} \right) - \Gamma \left(0.2, \frac{t}{0.0094} \right) \right\} \right]. \tag{23}$$

After vasodilation, with $\chi_v^4 = 2.17$ and $\chi_p^4 = 0.0625$, then

$$\sigma_{\text{SR}}(t) = \frac{A_0}{t^{0.2}} \left[\begin{aligned} &\frac{1}{2.17^{0.2}} \left\{ \Gamma \left(0.2, \frac{t}{(30\,000/2.17)} \right) - \Gamma \left(0.2, \frac{t}{(0.0003/2.17)} \right) \right\} \\ &+ \frac{1}{0.06^{0.2}} \left\{ \Gamma \left(0.2, \frac{t}{(940\,000/0.06)} \right) - \Gamma \left(0.2, \frac{t}{(0.0094/0.06)} \right) \right\} \end{aligned} \right]. \tag{24}$$

This result is shown in figure 6, along with a vasoconstriction case where $p/p_b = 0.6/0.7$, representing a modest 15% reduction in vessel sizes, compensated by a proportional increase in perivascular dimensions. These results are directly counter to the previous unconstrained examples of figures 2 and 3. This happens because in constrained-volume vasodilation there is a strong opposite effect of squeezing the perivascular fluid space to maintain constant fluid volume. The distribution of perivascular spaces is shifted to smaller dimensions, leading to longer time constants and a stiffening component that dominates the two parts (vascular/perivascular). On the other hand, a modest vasoconstriction simply allocates more space to the perivascular fluid and has only a small net overall effect.

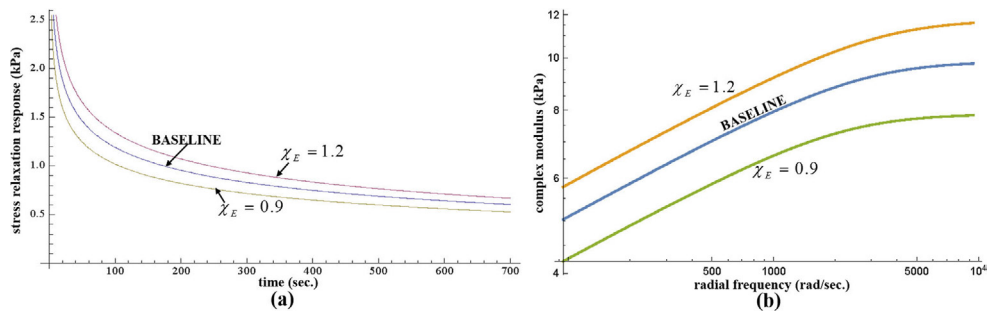


Figure 7. (a) Change in stress relaxation response assuming a 20% increase or decrease in the underlying elastic matrix due to electro-chemical-mechanical effects operating at a cellular and subcellular level. All vessel diameters remain constant in this example. (b) Magnitude of complex modulus vs. shear wave frequency from $2\pi 15$ Hz to $2\pi 1500$ Hz, for the baseline and electrochemical modulated elastic media. Generally, the results are proportional to the change seen in stress relaxation curves (7(a)), and are relatively consistent over the frequency range.

It should be noted, however, that the anomalous trend shown in figure 6 has a limited range. As p and χ increase during vasodilation, the outer annulus of figure 5 representing the perivascular space is ultimately closed off and unable to function as a fluid-carrying network. At this point, the second term of equation (20) is extinguished, and the presumably vasodilation-softening effect of figures 2 and 3 would then be observed. It must be emphasized that the results in this section are plausible only when local changes in the partitioning of the vascular/perivascular spaces are enabled by the flow of perivascular fluid into or out of that region.

2.5. Change in elastic matrix

Now consider the case where the elastic properties of the cellular structures change, without any alteration of vessel diameters. Electro-chemical effects in axons, dendritic spines, membranes, and even actin filaments have been reviewed by Tyler (2012) and Barnes (2017). Functional stimuli may incite regional electro-chemical changes (Patz *et al* 2016).

From equations (2) and (3) we see that some increase in the material’s stiffness E increases the stress relaxation force $\sigma_{SR}(t)$ but also changes the time constant τ for an idealized structural element subjected to uniaxial loading. However, the change in time constant is inversely proportional to E , and therefore is less sensitive than to changes in radius which has a $1/r^4$ dependence.

Again assuming a baseline case $E_b, A_b(\tau), \tau_{max}, \tau_{min}$, and $\sigma_{SR_b}(t)$, then if $E_2 = \chi_E E$ we can map the resulting changes through the transformation rules as derived in previous sections. Specifically, $\tau_2 = \tau/\chi_E, d\tau_2/d\tau = 1/\chi_E$:

$$\begin{aligned}
 A_2(\tau_2) &= \chi_E^2 A(\chi\tau_2) \\
 &= \frac{\chi_E^2 A_0}{(\chi_E \tau_2)^b} \\
 &= \frac{\chi_E^{(2-b)} A_0}{\tau_2^b},
 \end{aligned}
 \tag{25}$$

and after integrating:

$$\sigma_{SR2}(t) = \frac{\chi_E^{(2-b)} A_0 (\Gamma[a, t/\tau_{2max}] - \Gamma[a, t/\tau_{2min}])}{t^a}.
 \tag{26}$$

where $\tau_{2_{\max}} = \tau_{\max}/\chi_E$ and $\tau_{2_{\min}} = \tau_{\min}/\chi_E$.

Thus, an increase in E ($\chi_E > 1$) translates into two effects: an increase in the overall stress relaxation force by a factor of $\chi_E^{(2-b)}$, and a down-shifting of time constants by a factor of $1/\chi_E$, which has a slight ‘softening’ effect.

For the case of $\chi_E = 1.2$ (elastic modulus increases 20%) and $\chi_E = 0.9$ (decrease), see figure 7.

3. Discussion

It must be noted that the hypothetical scenarios presented have numerous assumptions and unknowns. All of the assumptions of the microchannel flow model are included, plus the treatment of the perivascular fluid space as the unique compensating compartment for vasodilation under the strict constraint of confined total volume. Furthermore, many of the parameters listed in table 1 and used in the scenarios are not well characterized; for example the baseline value of the ratio p that partitions the vascular to perivascular spaces. Finally, the theory considered herein are limited to isotropic and linear conditions. Brain anisotropy would produce a direction-dependent effect, which has been recently considered within the microchannel flow model (Parker 2017), and nonlinearities in tissues are thought to play a role during large displacements associated with elevated fluid pressures (Rotemberg *et al* 2012, Arani *et al* 2017).

With those caveats, the microchannel flow model predicts a strong response to vasomodulation in an unconfined organ. This effect has some experimental confirmation in other unconfined tissues, specifically vasoconstriction in the perfused placenta (McAleavey *et al* 2016) and in the excised liver after osmotic swelling (Parker 2015). However, under the constraints of a fixed total volume of the brain, the microchannel flow model uses the perivascular space as a compensating fluid volume. Of course, this presupposes that the perivascular fluid can drain into the subarachnoid space and beyond (figure 4), which is most likely for only localized vasodilation due to regional activation. Conversely, in the case of whole brain vasodilation, the squeezing of the entire perivascular space would result in an increased intracranial pressure (Czosnyka *et al* 2004) since there is no significant extra space available for the fluid to enter. This has been dramatically demonstrated in human subjects during carbogen breathing (Rich *et al* 1953), and represents a different physical condition from that supposed in section 2.

The electrochemical activation of regions of the brain by a variety of mechanisms (Tyler 2012) may have potential for creating changes in the observed elasticity (Patz *et al* 2016, Patz *et al* 2017b). By comparison, a different specialized tissue that has been studied extensively is lung tissue, where activation of different cell types can create dynamic changes (Yuan *et al* 1997), albeit limited, in measured elastic behavior (Suki *et al* 2011). They concluded that, ‘Stimulation of the contractile machinery of these cells with different agonists induces local internal stresses in the fiber network of the ECM that can lead to changes in the viscoelastic properties of the lung tissue. Nevertheless, the viscoelastic properties of the lung parenchyma are only moderately affected by the active tone of the interstitial cells’ (Suki *et al* 2011).

In section 2 we have primarily considered changes in complex modulus which would be assessed through shear wave speed or wavelength estimators in elastography experiments. Other parameters related to the lossy and frequency-dependent nature of viscoelastic materials include the loss tangent, the wave speed dispersion, and attenuation. In both the microchannel flow model and the Kelvin–Voigt fractional derivative models, these are all tightly linked (Parker 2014) to the power law parameter a , which is set to 0.2 in table 1 based on experience with a number of soft tissues (Zhang *et al* 2007, Parker *et al* 2016). In cases where a power law relationship has been specifically measured in brain, results cover a wide range from

$0.2 < a < 1.2$ (Streitberger *et al* 2011, Sack *et al* 2013, Testu *et al* 2017). Additional research is required to refine these estimates.

In the field of functional magnetic resonance imaging, (fMRI), the neuroactivation of a region followed by the vasoactive blood oxygenation level-dependent (BOLD) response (Malonek *et al* 1997, Buxton *et al* 1998, Hoge *et al* 1999, Sheth *et al* 2004) are present, and in the microchannel flow model scenarios contained in this paper, this mechanism (vasomodulation) and/or cellular matrix stiffness chemo-modulation could lead to a dynamic and localized increase in measures of ‘stiffness’. How can these different hypothetical effects be examined individually? Teasing out the baseline parameters and different mechanisms will require experimentation under a range of different conditions. For example, different types of anesthetics can have different effects on vasodilation, as can the mix of oxygen and carbon dioxide (Rich *et al* 1953, Czosnyka *et al* 2004). Neural activation and non-activation can be tested, these are already common within many fMRI protocols. In animal experiments, independent measurements of regional blood flow and perivascular flow will be helpful. Ultimately, the empirical findings in humans will set the expected values for stiffness measurements in normal and pathological conditions, however any dynamic response must be either controlled or elicited and measured as part of the experimental protocols.

4. Conclusion

The brain is a unique organ in many respects and could have dynamic elastic behaviors that are not replicated in other organs. The microchannel flow model predicts an increased σ_{SR} and SWS produced by vasoconstriction (in an unconfined volume), by increasing the E of the cellular matrix by electro-chemical activation, or by vasodilation in a confined space where extra-vascular (perivascular) spaces are squeezed to compensate. Decreased σ_{SR} and SWS are produced in the converse cases. These effects are dynamic and can be frequency-dependent, thus careful experimental controls are required to determine their relative magnitude and associated time constants.

Acknowledgments

This work was supported by the Hajim School of Engineering and Applied Sciences at the University of Rochester. The author is grateful to Professor Sam Patz for his insightful comments on MRE activation experiments.

Appendix

In modeling the effects of the perivascular space on the elastic behavior of the brain, a simplifying assumption was made. The annulus formed by Δr extending from r_{\min} to pr_{\max} is treated in section 2.4, using the microchannel flow model, as equivalent to a vessel of radius $\Delta r = r_{\max}(1-p)$. This would be reasonable if the flow Q is proportional to Δr^4 as in equations (1)–(3), which set the underlying rationale for the microchannel flow model.

However the laminar flow in an annulus is given by Rosenhead (1963):

$$Q = \frac{\Delta P \pi}{L 8 \mu} \left[(r_{\max}^4 - pr_{\max}^4) - \frac{(r_{\max}^2 - pr_{\max}^2)}{\ln\left(\frac{1}{p}\right)} \right] = \frac{\Delta P \pi r_{\max}^4}{L 8 \mu} \left[(1 - p^4) - \frac{(1 - p^2)^2}{\ln\left(\frac{1}{p}\right)} \right], \quad (\text{A.1})$$

whereas for a cylindrical vessel (pipe) of radius $r_{\max}(1-p)$ the conventional Hagen-Poiseuille's law yields:

$$Q = \frac{\Delta P \pi}{L 8 \mu} r_{\max}^4 (1-p)^4. \quad (\text{A.2})$$

The two expressions are not close except near $p \rightarrow 1$ where $Q \rightarrow 0$. A Taylor series expansion of equation (A.1) with respect to p near $p = 1$ yields a $r_{\max}^4(1-p)^3$ term and a $r_{\max}^4(1-p)^4$ term, and higher orders which are not significant in our range of interest ($0.8 < p < 1$). Thus, the more accurate modeling of the behavior of an annular fluid space like the perivascular space would require a re-derivation of the microchannel flow model beginning with both a $r_{\max}^4(1-p)^3$ and a $r_{\max}^4(1-p)^4$ term in equation (1). The consequences of this mixed power law are left for future research.

References

- Arani A, Min H K, Fattahi N, Wetjen N M, Trzasko J D, Manduca A, Jack C R Jr, Lee K H, Ehman R L and Huston J III 2017 Acute pressure changes in the brain are correlated with MR elastography stiffness measurements: initial feasibility in an in vivo large animal model *Magn. Reson. Med.* (<https://doi.org/10.1002/mrm.26738>)
- Barnes J M, Przybyla L and Weaver V M 2017 Tissue mechanics regulate brain development, homeostasis and disease *J. Cell Sci.* **130** 71–82
- Buxton R B, Wong E C and Frank L R 1998 Dynamics of blood flow and oxygenation changes during brain activation: the balloon model *Magn. Reson. Med.* **39** 855–64
- Chan H W, Pressler R, Uff C, Gunny R, St Piers K, Cross H, Bamber J, Dorward N, Harkness W and Chakraborty A 2014 A novel technique of detecting MRI-negative lesion in focal symptomatic epilepsy: intraoperative ShearWave elastography *Epilepsia* **55** e30–3
- Chauvet D, Imbault M, Capelle L, Demene C, Mossad M, Karachi C, Boch A L, Gennisson J L and Tanter M 2016 *In vivo* measurement of brain tumor elasticity using intraoperative shear wave elastography *Ultraschall Med.* **37** 584–90
- Czosnyka M, Czosnyka Z, Momjian S and Pickard J D 2004 Cerebrospinal fluid dynamics *Physiol. Meas.* **25** R51–76
- Desmidt T, Hachemi M E, Remenieras J P, Lecomte P, Ferreira-Maldent N, Patat F and Camus V 2011 Ultrasound brain tissue pulsatility is decreased in middle aged and elderly type 2 diabetic patients with depression *Psychiatry Res.* **193** 63–4
- Ferry J D 1970 *Viscoelastic Properties of Polymers* (New York: Wiley) ch 1
- Fox P T and Raichle M E 1986 Focal physiological uncoupling of cerebral blood flow and oxidative metabolism during somatosensory stimulation in human subjects *Proc. Natl Acad. Sci. USA* **83** 1140–4
- Fung Y C 1981 *Biomechanics: Mechanical Properties of Living Tissues* (New York: Springer) ch 2
- Harnarine-Singh D, Geddes G and Hyde J B 1972 Sizes and numbers of arteries and veins in normal human neopallium *J. Anat.* **111** 171–9
- Hiscox L V, Johnson C L, Barnhill E, McGarry M D, Huston J, van Beek E J, Starr J M and Roberts N 2016 Magnetic resonance elastography (MRE) of the human brain: technique, findings and clinical applications *Phys. Med. Biol.* **61** R401–37
- Hoge R D, Atkinson J, Gill B, Crelier G R, Marrett S and Pike G B 1999 Investigation of BOLD signal dependence on cerebral blood flow and oxygen consumption: the deoxyhemoglobin dilution model *Magn. Reson. Med.* **42** 849–63
- Lakes R S 1999 *Viscoelastic Solids* (Boca Raton, FL: CRC Press) ch 2
- Malonek D, Dirnagl U, Lindauer U, Yamada K, Kanno I and Grinvald A 1997 Vascular imprints of neuronal activity: relationships between the dynamics of cortical blood flow, oxygenation, and volume changes following sensory stimulation *Proc. Natl Acad. Sci. USA* **94** 14826–31
- McAleavey S A, Parker K J, Ormachea J, Wood R W, Stodgell C J, Katzman P J, Pressman E K and Miller R K 2016 Shear wave elastography in the living, perfused, post-delivery placenta *Ultrasound Med. Biol.* **42** 1282–8

- Møller M, Møllgård K, Lund-Andersen H and Hertz L 1974 Concordance between morphological and biochemical estimates of fluid spaces in rat brain cortex slices *Exp. Brain Res.* **21** 299–314
- Ormachea J, Lavarello R J, McAleavey S A, Parker K J and Castaneda B 2016 Shear wave speed measurements using crawling wave sonoelastography and single tracking location shear wave elasticity imaging for tissue characterization *IEEE Trans. Ultrason. Ferroelectr. Freq. Control* **63** 1351–60
- Papoulis A 1987 *The Fourier Integral and Its Applications* (New York: McGraw-Hill)
- Parker K J 2014 A microchannel flow model for soft tissue elasticity *Phys. Med. Biol.* **59** 4443–57
- Parker K J 2015 Experimental evaluations of the microchannel flow model *Phys. Med. Biol.* **60** 4227–42
- Parker K J 2017 The microchannel flow model under shear stress and higher frequencies *Phys. Med. Biol.* **62** N161–7
- Parker K J, Doyley M M and Rubens D J 2011 Imaging the elastic properties of tissue: the 20 year perspective *Phys. Med. Biol.* **56** R1–29
- Parker K J, Ormachea J, McAleavey S A, Wood R W, Carroll-Nellenback J J and Miller R K 2016 Shear wave dispersion behaviors of soft, vascularized tissues from the microchannel flow model *Phys. Med. Biol.* **61** 4890–903
- Patz S, Nazari N, Barbone P, Fabry B, Fovargue D, Nordsletten D and Sinkus R 2017a Functional neuroimaging in the brain using magnetic resonance elastography *25th Annual Int. Society for Magnetic Resonance Medicine (Honolulu, HI, USA)* p 242 (Abstract)
- Patz S, Nazari N, Barbone P E and Sinkus R 2016 Functional changes in cortical stiffness observed with magnetic resonance elastography *Proc. of the 15th Int. Tissue Elasticity Conf. (Lake Morey, VT, USA)* p 53
- Patz S, Nazari N, Schregel K, Palotai M, Barbone P E and Sinkus R 2017b Functional neuro-imaging with magnetic resonance elastography *J. Acoust. Soc. Am.* **141** 3492
- Rich M, Scheinberg P and Belle M S 1953 Relationship between cerebrospinal fluid pressure changes and cerebral blood flow *Circ. Res.* **1** 389–95
- Risser L, Plouraboue F, Steyer A, Cloetens P, Le Duc G and Fonta C 2007 From homogeneous to fractal normal and tumorous microvascular networks in the brain *J. Cerebr. Blood Flow Metab.* **27** 293–303
- Rosenhead L 1963 *Laminar Boundary Layers* (Oxford: Clarendon)
- Rotemberg V, Palmeri M, Nightingale R, Rouze N and Nightingale K 2012 The impact of hepatic pressurization on liver shear wave speed estimates in constrained versus unconstrained conditions *Phys. Med. Biol.* **57** 329–41
- Sack I, Johrens K, Wurfel J and Braun J 2013 Structure-sensitive elastography: on the viscoelastic powerlaw behavior of *in vivo* human tissue in health and disease *Soft Matter* **9** 5672–80
- Sheth S A, Nemoto M, Guiou M, Walker M, Pouratian N and Toga A W 2004 Linear and nonlinear relationships between neuronal activity, oxygen metabolism, and hemodynamic responses *Neuron* **42** 347–55
- Streitberger K J, Wiener E, Hoffmann J, Freimann F B, Klatt D, Braun J, Lin K, McLaughlin J, Sprung C, Klingebiel R and Sack I 2011 *In vivo* viscoelastic properties of the brain in normal pressure hydrocephalus *NMR Biomed.* **24** 385–92
- Suki B, Stamenovic D and Hubmayr R 2011 Lung parenchymal mechanics *Compr. Physiol.* **1** 1317–51
- Sutera S P 1993 The history of Poiseuille's law *Annu. Rev. Fluid Mech.* **25** 1–19
- Ternifi R, Cazals X, Desmidt T, Andersson F, Camus V, Cottier J P, Patat F and Remenieras J P 2014 Ultrasound measurements of brain tissue pulsatility correlate with the volume of MRI white-matter hyperintensity *J. Cerebr. Blood Flow Metab.* **34** 942–4
- Testu J, McGarry M D J, Dittmann F, Weaver J B, Paulsen K D, Sack I and Van Houten E E W 2017 Viscoelastic power law parameters of *in vivo* human brain estimated by MR elastography *J. Mech. Behav. Biomed. Mater.* **74** 333–41
- Tyler W J 2012 The mechanobiology of brain function *Nat. Rev. Neurosci.* **13** 867–78
- West G B, Brown J H and Enquist B J 1997 A general model for the origin of allometric scaling laws in biology *Science* **276** 122–6
- Yuan H, Ingenito E P and Suki B 1997 Dynamic properties of lung parenchyma: mechanical contributions of fiber network and interstitial cells *J. Appl. Physiol.* **83** 1420–31
- Zhang E T, Inman C B E and Weller R O 1990 Interrelationships of the pia mater and the perivascular (Virchow–Robin) spaces in the human cerebrum *J. Anat.* **170** 111–23
- Zhang M, Castaneda B, Wu Z, Nigwekar P, Joseph J V, Rubens D J and Parker K J 2007 Congruence of imaging estimators and mechanical measurements of viscoelastic properties of soft tissues *Ultrasound Med. Biol.* **33** 1617–31